Non-linear steady states in dense granular flows

Daniel Bonamy, Pierre-Henri Chavanis, François Daviaud, Bérengère Dubrulle, Mathieu Renouf

▶ **To cite this version:**

Daniel Bonamy, Pierre-Henri Chavanis, François Daviaud, Bérengère Dubrulle, Mathieu Renouf. Non-linear steady states in dense granular flows. 2008. hal-00260015v1

HAL Id: hal-00260015
https://hal.science/hal-00260015v1

Preprint submitted on 2 Mar 2008 (v1), last revised 5 Mar 2016 (v2)

HAL is a multi-disciplinary open access archive for the deposit and dissemination of scientific research documents, whether they are published or not. The documents may come from teaching and research institutions in France or abroad, or from public or private research centers.

L'archive ouverte pluridisciplinaire **HAL**, est destinée au dépôt et à la diffusion de documents scientifiques de niveau recherche, publiés ou non, émanant des établissements d'enseignement et de recherche français ou étrangers, des laboratoires publics ou privés.

Non-linear steady states in dense granular flows

D. Bonamy,[1] P. H. Chavanis,[2] F. Daviaud,[3] B. Dubrulle,[3] and M. Renouf[4]

[1] *Groupe fracture, DSM/DRECAM/SPCSI, CEA Saclay, F-91191 Gif sur Yvette - France*
[2] *Laboratoire de Physique Théorique (UMR 5152), Université Paul Sabatier, 118, route de Narbonne 31062 Toulouse, France*
[3] *Groupe Instabilité & Turbulence, DSM/DRECAM/SPEC, CEA Saclay, F-91191 Gif sur Yvette - France*
[4] *Equipe TMI - LaMCoS/INSA Lyon - UMR5259, 18-20 rue des sciences, F-69621 Villeurbannes - France*

(Dated: March 3, 2008)

General conservation equations are derived for 2D dense granular flows within the Boussinesq approximation. Assuming that forcing and dissipation equilibrate on average, the relationships between local granular temperature, vorticity and stream function are shown to be characterized by two functions. Once these two functions are known, the whole velocity and temperature fields can be deduced. We checked these predictions on steady surface flows in rotating drum simulated through the Non-Smooth Contact Dynamics methods. Also, we briefly discuss some possible ways to derive these two functions using statistical mechanics.

PACS numbers: 45.70.-n, 83.70.Fn, 46.10.+z

hal-00260015, version 1 - 2 Mar 2008

I. INTRODUCTION

The intrinsic dissipative nature of the interactions between the constituent macroscopic particles sets granular media apart from conventional solids, liquids and gases [1]. Understanding the rheology of granular systems is thus rather difficult. Depending on the flow velocity, three regimes are usually distinguished: The *rapid flow* – gaseous-like – regime where grains interact through binary collisions, is generally described within the framework of the kinetic theory [2, 3, 4]; The *slow flow* – solid-like – regime, where grain inertia is negligible, is most commonly described using the tools of soil mechanics and plasticity theory [5]. In between these two regimes there exists a *dense flow* – liquid-like – regime where grain inertia becomes important but contacts between grains are still relevant. This last regime has been widely investigated experimentally, numerically and theoretically (see [6] for a review) in various flow configurations. Several constitutive laws have been derived by accounting for non-local effects [7, 8, 9, 10, 11], by adapting kinetic theory [12, 13, 14], by modelling dense flows as partially fluidized flows [15], by considering them as quasi-static flows where the mean motion results from transient fractures modelled as self activated process [16, 17, 18, 19] or more recently by considering them as visco-plastic fluids [20, 21, 22]. To our knowledge, all these approaches fail to account for all the features experimentally observed. In some sense, similar difficulties are encountered in the understanding and modelling of turbulent fluids. In that case, the challenge is to relate the Reynolds stresses, based on small scale fluctuations, to large scale or time averaged quantities. A new way to tackle this problem was recently suggested [23, 24, 25], through the consideration of non-linear steady solutions of the Euler equations, thereby disregarding any non-universal effects induced by (large scale) forcing and (small scale) dissipation. When applied to a turbulent von Karman flow, this approach leads to the characterization of the steady state velocities through two functions, encoding all information about the forcing and the dissipation. In the present paper, this method is generalized to the case of inhomogeneous dense granular flows. As a result, one obtains a characterization of the steady state through two general functions that relate granular temperature, granular vorticity and granular stream function. In other words, the knowledge of these two functions is sufficient to fully reconstruct the two-dimensional (2D) field of velocity, granular temperature, and volume fraction.

The paper is organized as follows: In Sec. II, the structure of 2D steady granular surface flows is derived in the rotating drum geometry. Hydrodynamics and state equations in granular media are briefly discussed in Sec. IIA. Conservation equations are then rewritten assuming that volume fraction is nearly constant within the flow (Boussinesq approximation) in Sec. IIB, and then in the force-free, inviscid limit in Sec. IIC. The general shape of the stationary solutions within this limit is given in Sec. IID. In particular, it is shown that these states can be fully characterized through the knowledge of two functions F and G. Section III confronts these predictions with steady surface flows in rotating drum as obtained in Contact Dynamics simulations reported in [26] that were shown to reproduce the experimental features observed in Refs. [27, 28, 29]. The simulation scheme and the description of the simulated systems are briefly recalled in Sec. IIIA. Spatial distribution of the averaged temperature, volume fraction, vorticity and stream function fields are determined within the whole drum, at the grain scale (Sec. IIIB). The two characteristic functions F and G are then determined from the numerical experiments (Sec. IIIC) and commented (Sec. IIID). In the last section of this paper (Sec. IV) some possible ways to derive these two functions are briefly discussed.

II. THEORETICAL FRAMEWORK: CONSERVATION EQUATIONS WITHIN THE BOUSSINESQ APPROXIMATION

A. Granular hydrodynamics

It is commonly assumed that granular media can be described with continuum models. The mass, momentum and energy conservation equations then lead to:

$$\begin{aligned}\partial_t \nu + \nabla\cdot(\nu\mathbf{v}) &= 0,\\ \partial_t \nu\mathbf{v} + (\mathbf{v}\cdot\nabla)\,\nu\mathbf{v} &= -\nabla P + \nu\mathbf{g} + \mathbf{F}_{visc} + \mathbf{F}_{forc},\\ \partial_t \nu T + \nabla\cdot(\nu T\mathbf{v}) &= -P\nabla\cdot\mathbf{v} + E_{visc} + E_{forc}. \end{aligned} \quad (1)$$

In these equations, $\nu(x,z,t)$ is the field of volume fraction, $\mathbf{v}(x,z,t)$ the velocity field; $\mathbf{g}$ is the gravitational acceleration; $T(x,z,t)$ is the field of granular temperature defined in term of the RMS part of the velocity field, $T(x,z,t) = \frac{1}{2}\langle(\mathbf{c}_b(t)-\mathbf{v}(x,z,t))^2\rangle_{b\in(x,z)}$ where $\mathbf{c}_b(t)$ refers to the instantaneous velocity of the bead b located at time t within the elementary volume located in (x,z); $\mathbf{F}_{forc}$, E_{forc} stand for external forcing and $\mathbf{F}_{visc}$, E_{visc} stand for all dissipative processes. This system has to be supplemented by an equation of state $P = g(\nu)T$ and rheology, i.e. some constitutive equations describing the dissipative processes $\mathbf{F}_{visc}$, E_{visc}.

Contrary to classical liquids, the density and temperature dependence of transport coefficients play an important role in determining the flow density. For dilute systems they are usually obtained using kinetic theory of granular gases [2, 3, 4] within the Enskog approximation. For dense gases, there is no available systematic theory allowing their description. They are therefore usually prescribed using phenomenological models [13] or fitted using experimental [21, 22, 30] or numerical [31] data. In particular, the equation of state can be written in the high-density limit [21, 31]:

$$P \simeq K\frac{\nu_*^2}{\nu_*-\nu}T, \quad (2)$$

where K is a constant and ν_* the random closed packed limit: $\nu_* \simeq 0.82$ for 2D packing and $\nu_* \simeq 0.64$ for 3D packings. At $\nu = \nu_*$ this equation therefore predicts a zero granular temperature, consistent with the absence of motion.

As for the dissipative terms and forcing, their precise shape shall not be needed in the sequel. This is a distinguished feature of our approach.

B. The Boussinesq approximation

For simplicity, one focuses on situations where the volume fraction is nearly constant close to the random closed packed limit $\nu \approx \nu_*$. In the considered system, this approximation is satisfied within 10 percent. Generalization to non constant volume fraction is possible, but more involved. In that limit, the classical Boussinesq approximation is implemented by neglecting the fluctuation of volume fraction in the continuity equation so that it becomes:

$$\nabla\cdot\mathbf{v} \approx 0. \quad (3)$$

The other conservation equations may then be simplified by defining a reference state with $\mathbf{v} = 0$, $T = 0$, $P = P_*$, $\nu = \nu_*$, so that:

$$\nabla P_* = \nu_*\mathbf{g}, \quad (4)$$

i.e. an hydrostatic equilibrium in the vertical direction. Along with non-zero velocity, we introduce temperature and volume fraction deviations with respect to the reference state, as:

$$\nu = \nu_* - \delta\nu; \quad T = \delta T; \quad P = P_* + \delta P. \quad (5)$$

The momentum equation can then be written as:

$$\begin{aligned}\partial_t\mathbf{v} + (\mathbf{v}\cdot\nabla)\,\mathbf{v} &= -\frac{1}{\nu}\nabla P + \mathbf{g} + \mathbf{F}_{visc} + \mathbf{F}_{forc},\\ &\approx -\frac{1}{\nu_*}\nabla\delta P - \frac{\delta\nu}{\nu_*^2}\nabla P_* + \mathbf{g} - \frac{1}{\nu_*}\nabla P_*\\ &\quad + \mathbf{F}_{visc} + \mathbf{F}_{forc},\\ &= -\frac{1}{\nu_*}\nabla\delta P - \frac{\delta\nu}{\nu_*}\mathbf{g} + \mathbf{F}_{visc} + \mathbf{F}_{forc}, \end{aligned} \quad (6)$$

where the hydrostatic equilibrium has been used to simplify the last equation. A similar treatment of the temperature equation leads to:

$$\partial_t\delta T + (\mathbf{v}\cdot\nabla)\,\delta T = E_{visc} + E_{forc} - \frac{P_*}{\nu_*}\nabla\cdot\mathbf{v} \approx E_{visc} + E_{forc}. \quad (7)$$

The system of resulting equations can be further transformed so that it involves only temperature fluctuation by using Eq. 2:

$$\frac{\delta\nu}{\nu_*} = \left(\frac{\delta T}{T_{ref}}\right), \quad (8)$$

where the reference temperature field $T_{ref}(\mathbf{r})$ is given by $T_{ref} = P_*/K\nu_*$, so that $\mathbf{g} = K\nabla T_{ref}$, and only the first order terms in $\delta\nu/\nu_*$, $\delta T/T_{ref}$ and $\delta P/P_*$ are kept. The system of equations of the weakly compressible granular medium then takes the shape:

$$\begin{aligned}&\nabla\cdot\mathbf{v} = 0,\\ &\partial_t\mathbf{v} + (\mathbf{v}\cdot\nabla)\,\mathbf{v} = -\frac{1}{\nu_*}\nabla\cdot\delta P - \left(\frac{\delta T}{T_{ref}}\right)\mathbf{g} + \mathbf{F}_{visc} + \mathbf{F}_{forc},\\ &\partial_t\delta T + (\mathbf{v}\cdot\nabla)\,\delta T = E_{visc} + E_{forc}. \end{aligned} \quad (9)$$

Note that the system can also be formulated in a more classical Boussinesq-like equation by introducing the

variable $\theta = \delta T/T_{ref}$ and noting that T_{ref} is not a constant (it varies along the gravity direction), so that:

$$\begin{aligned}
&\nabla \cdot (\mathbf{v}) = 0, \\
&\partial_t \mathbf{v} + (\mathbf{v}\cdot\nabla)\,\mathbf{v} = -\frac{1}{\nu_*}\nabla\cdot\delta P - \theta\mathbf{g} + \mathbf{F}_{visc} + \mathbf{F}_{forc}, \\
&\partial_t\theta + (\mathbf{v}\cdot\nabla)\,\theta + (\mathbf{v}\cdot\nabla)\log T_{ref} = E_{visc} + E_{forc}. \quad (10)
\end{aligned}$$

In the sequel, we shall however rather work with the formulation (9).

C. 2D case

We now specialize our granular hydrodynamics to the case of 2D medium, such as flow within a thin rotating drum of diameter $2R$, rotated along the y axis at a constant angular velocity Ω as investigated in Sec. III. If the width of the drum in the y direction is thin with respect to the characteristic length scale of (x, z) motions, the velocity field can be assumed two-dimensional $\mathbf{v}(x, z, t)$. In that case, the vorticity is directed along the y axis and the forcing is supplied by the boundary conditions. In that case, one can recast Eq.9 in cartesian coordinates (x, z) as:

$$\begin{aligned}
\partial_x v_x + \partial_z v_z &= 0\,, \quad (11)\\
\partial_t v_x + v_x\partial_x v_x + v_z\partial_z v_x &= -\frac{1}{\nu_*}\partial_x\delta P - g_x\left(\frac{\delta T}{T_{ref}}\right) \\
&\quad + F^x_{visc} + F^x_{forc}\,, \\
\partial_t v_z + v_x\partial_x v_z + v_z\partial_z v_z &= -\frac{1}{\nu_*}\partial_z\delta P - g_z\left(\frac{\delta T}{T_{ref}}\right) \\
&\quad + F^z_{visc} + F^z_{forc}\,, \\
\partial_t\delta T + v_x\partial_x\delta T + v_z\partial_z\delta T &= E_{visc} + E_{forc}\,, \quad (12)
\end{aligned}$$

where (v_x, v_z) (resp. (g_x, g_z)) denote the components of the velocity field (resp. gravity field) in a cartesian referential. Note that the third equation expresses the conservation of the granular temperature δT. The two other equations for v_x and v_z involve a pressure field determined through incompressibility. However, it can be eliminated by using the stream function ψ defined by:

$$v_x = \partial_z\psi, \qquad \text{and} \qquad v_z = -\partial_x\psi\,.$$

The existence of a stream function results from the incompressibility and the 2D nature of the flow. Calling q the y-component of the vorticity, one gets:

$$q = \partial_z v_x - \partial_x v_z = \Delta\psi. \quad (13)$$

where $\Delta\psi = \partial_x^2\psi + \partial_z^2\psi$ is the Laplacian. Taking the curl of the equation for velocity, the equations (12) can be recast as:

$$\begin{aligned}
\partial_t\delta T + \{\psi, \delta T\} &= E_{visc} + E_{forc}\,, \quad (14)\\
\partial_t q + \{\psi, q\} &= K\{\log T_{ref}, \delta T\} + \nabla\times(\mathbf{F}_{visc} + \mathbf{F}_{forc})
\end{aligned}$$

where $\{\psi, \phi\} = \partial_z\psi\partial_x\phi - \partial_x\psi\partial_z\phi$ is the Jacobian. The relation between gravity and T_{ref} was also used to simplify the buoyancy term. This formulation of the stratified Navier-Stokes equation has to be supplemented by appropriate boundary conditions. Notice that only two scalar fields are sufficient to describe the flows under consideration: δT, the granular temperature and q, the y-component of the vorticity.

D. Steady state solutions

Consider now situations where forcing and dissipation equilibrate on average: $\overline{\mathbf{F}_{visc} + \mathbf{F}_{forc}} = \overline{E_{visc} + E_{forc}} = 0$, so that one gets steady flows. This situation is the one commonly realized in rheometric experiments when one imposes a given and tuneable forcing $\mathbf{F}_{forc}$, E_{forc} to get a measured steady velocity profile $\mathbf{v}$. Variations of $\mathbf{v}$ with respect to *forc* allows then to find the rheology of the studied materials, i.e. the relations between the dissipative terms $\mathbf{F}_{visc}$, E_{visc} and the deformation rate.

Here, we focus on the left-hand side of Eqs. 14 to see the implications of making $\overline{\mathbf{F}_{visc} + \mathbf{F}_{forc}} = \overline{E_{visc} + E_{forc}} = 0$ on the form taken by the fields ψ, q and δT. The steady states then obey the averaged equations:

$$\begin{aligned}
\overline{\{\psi, \delta T\}} &= 0\,, \quad (15)\\
\overline{\{\psi, q\}} &= K\{\log T_{ref}, \overline{\delta T}\}.
\end{aligned}$$

Neglecting fluctuations $\overline{\{\psi, \delta T\}} \approx \{\bar\psi, \overline{\delta T}\}$, one gets:

$$\begin{aligned}
\{\psi, \delta T\} &= 0\,, \quad (16)\\
\{\psi, q\} &= K\{\log T_{ref}, \delta T\}\,,
\end{aligned}$$

where the overlines over q, T and ψ are now omitted for sake of simplicity. The first equation is satisfied if

$$\delta T = F(\psi), \quad (17)$$

where F is an arbitrary function. Using the general identity

$$\{f, h(g)\} = h'(g)\{f, g\} = \{h'(g)f, g\}, \quad (18)$$

Where f, g and h are arbitrary functions, the second equation becomes

$$\{\psi, q + F'(\psi)K\log T_{ref}\} = 0. \quad (19)$$

Therefore, the general stationary solution of Eqs. (14) is of the form

$$\delta T = F(\psi) \quad \text{and} \quad q + KF'(\psi)\log T_{ref} = G(\psi), \quad (20)$$

Where F and G are arbitrary functions. Recalling the connection between q and ψ, one can therefore characterize the stationary states through the two function F and G as:

$$\begin{aligned}
\delta T &= F(\psi), \\
\Delta\psi = q &= -KF'(\psi)\log T_{ref} + G(\psi). \quad (21)
\end{aligned}$$

It should be emphasized that the functions F and G depend on the forcing and dissipation. Indeed, the competition between these two effects are responsible for the selection of the precise shape for F and G. But once these functions are known, one can solve the second equation of (21) to get ψ as a function of x and z, and then derive from this expression the temperature and velocity profile. To close the system of conservation equations, it is then sufficient to give the expression for F and G. There are probably several ways to prescribe these functions. For example, one could use a statistical mechanics approach in order to select the "most probable" form of these functions depending on microscopic constraints, using methods of information theory (see e.g. refs. [23, 24, 32, 33] for illustrations in turbulence). One could also follow the procedure used in rheology studies, and try to define these functions through "minimal" experimental or numerical measurements performed on the considered system.

III. APPLICATION TO SIMULATED STEADY SURFACE FLOWS

The formalism described in the previous section is now applied to the inhomogeneous steady surface flows observed in rotating drums.

A. Simulation methodology

The simulations have been performed using Non-Smooth Contact Dynamics approach [34, 35]. The algorithms benefit from parallel versions [36, 37] which show their efficiency in the simulation of large systems. The scheme has been described in detail elsewhere [26] and is briefly recalled below: An immobile drum of diameter $D_0 = 45$ cm is half-filled with 7183 rigid disks of density $\rho_0 = 2.7$ g.cm^{-3} and diameter uniformly distributed between 3 and 3.6 mm. The weak polydispersity introduced in the packing prevents 2D ordering effects. The normal restitution coefficient between two disks (resp. between disks and drum) is set to 0.46 (resp. 0.46) and the friction coefficient to 0.4 (resp. 0.95). Once the packing is stabilized, a constant rotation speed ranging from 2 to 15 rpm is imposed to the drum. After one round, a steady continuous surface flow is reached. One starts then to capture 400 snapshots equally distributed over a rotation of the drum.

For each bead of each of the 400 frames within a given numerical experiment, one records the position $\mathbf{r}$ of its center of mass and the "instantaneous" velocity $\mathbf{c}$ averaged over the time step $\delta t = 6 \times 10^{-3}$ s of the simulation. The frame $\Re$ is defined as the frame rotating with the drum that coïncides with the reference frame $\Re_0 = (\mathbf{e}_x, \mathbf{e}_z)$ fixed in the laboratory so that $\mathbf{e}_x$ (resp. $\mathbf{e}_z$) is parallel (resp. perpendicular) to the free surface (Fig. 1). The drum is then divided into elementary square cells $\Sigma(x, z)$ of size set equal to the mean bead diameter. The continuum time-averaged field $\bar{a}(x, z)$ at a position (x, z) is then defined as the average of the corresponding quantity defined at the grain scale over all the beads in all the 400 frames of the sequence whose center of mass is within the cell located in (x, z). Figure 1 shows the spatial distribution of the x-component of the time-averaged velocity field $\mathbf{v}(x, z)$as obtained within this procedure. The flowing layer and the static phase are then defined as the point where v_x is above and below a threshold value arbitrary chosen to 0.2. Let us note that all the results presented below do not depend on this threhold value. The interface between the two phases as defined within this procedure is represented as a black line in Fig. 1.

B. Spatial distribution of the relevant continuous fields within the drum

Let us first determine the granular temperature field within the drum. Calling $\mathbf{c}_i(t)$ the instantaneous velocity of a bead i at a given time t, the fluctuating part of the velocity $\delta\mathbf{c}_i(t)$ is defined as $\delta\mathbf{c}_i(t) = \mathbf{c}_i(t) - \mathbf{v}(x, z)$ where $\mathbf{v}(x, z)$ is the mean velocity value on the cell $\Sigma(x, z)$ that contains the bead i. One can then associate a granular temperature $T_i(t) = \frac{1}{2}\delta c_i^2(t)$ to the considered bead. Figure 2a shows a typical snapshot of the instantaneous temperature distribution within the drum as obtained using this procedure. Two phases can be clearly distinguished. Within the static phase, the temperature is very close to zero. Within the flowing layer, the spatial distribution of instantaneous local temperature shows large fluctuations, with hot and cold spots gathered in transient clusters of various sizes. This structure of hot/cold aggregates probably has its origin in the existence of "jammed" aggregates embedded in the flow, as evidenced in rotating drum experiments [38]. Since we are primarily interested in steady averaged fields in relation with the theoretical framework developed in Sec. II, we focus on the spatial distribution of the temperature after averaging over the 400 snapshots of the sequence. The corresponding time-averaged temperature field is represented in Fig. 2b.

Voronoï tessellation is then used to associate an instantaneous elementary volume as defined in Continuum Mechanics to each bead i on each snapshot (see *e.g.* [26] for related discussion). Calling A_i the area of the Voronoï polyhedra enclosing the grain i, the instantaneous volume fraction ν_i is defined as $\nu_i = \pi d_i^2/4A_i$ where d_i denotes the diameter of bead i. Typical snapshot of the resulting instantaneous map of volume fraction is presented in Fig. 2c. Apart from a very narrow region – about one bead diameter wide – at the free surface and along the drum boundary, the volume fraction appears almost constant, around $\langle\nu\rangle \simeq 0.82$, with apparent random fluctuations with standard deviation $\langle\nu^2\rangle - \langle\nu\rangle^2 \simeq 0.04$. However, the time-averaged field of volume fraction presented in Fig. 2d reveals that ν decreases slightly within the flowing layer, as expected since dilatancy effects should accompany granular deformation [39].

To compute the instantaneous vorticity ω_i associated to each bead i of each snapshot at time t, the following procedure is adopted: (i) The Voronoï polygon associated with the bead i is dilated homothetically by a factor two, so that each edge goes through one of the neighbouring beads; (ii) the circulation $\Gamma_i(t) = \sum_j \mathbf{c}_j(t).\mathbf{s}_j(t)$ is calculated around the resulting polygon - each point of a given segment $\mathbf{s}_j$ is assumed to have a constant velocity $\mathbf{c}_j(t)$ equal to the one of the embedded bead; (iii) the instantaneous vorticity $\omega_i(t)$ is then defined as $q_i(t) = \Gamma_i(t)/A_i(t)$ where $A_i(t)$ refers to the area of the initial Voronoï polygon.

Typical snapshot of the instantaneous vorticity distribution within the drum as obtained using this procedure is presented in Fig. 2e. This distribution is complex. It exhibits large fluctuations that self-organize into transient network of 1D chains. The characterization of this transient structure is postponed to future work. Figure 2f presents the time averaged vorticity field in the drum for $\Omega = 6$ rpm.

The last continuous field of interest in relation with the theoretical framework presented in Sec. II is the stream function $\psi(x, z)$. Its value is set to $\psi = 0$ at the drum boundary. The value $\psi(x, z)$ is then defined as the flow rate going through a line connecting the point M at position $\mathbf{r}(x, z)$ to any point at the drum boundary like *e.g.* point M_0 at position $\mathbf{r}_0(x, -\sqrt{D_0^2/4 - x^2})$:

$$\psi(x,z) = \int_{-\sqrt{D_0^2/4-x^2}}^{z} \nu(x,u)v_x(x,u)\mathrm{du} \qquad (22)$$

where $\nu(x, z)$ and $v_x(x, z)$ denote the field of volume fraction and x-component of velocity computed before. The resulting spatial distribution of stream function is shown in Fig. 3.

C. Determination of the two closure functions within Boussinesq approximation

Let us first determine the value of the parameters K and ν_* involved in the equation of state given by Eq. 2. This determination requires the pressure field P_* in the reference frame, when $\mathbf{v} = \mathbf{0}$. From Eq. 4, one gets $P_*(x, z) = -z\nu_* \cos\theta$ where θ is the slope of the free surface. Equation 8 can then be rewritten as:

$$\nu(x,z) = \nu_* + K\nu_* \frac{T(x,z)}{z\cos\theta} \qquad (23)$$

The time-averaged local volume fraction $\nu(x, z)$ is plotted as a function of the ratio $T(x, z)/z\cos\theta$ in Fig. 4. The values of both ν_* and K can then be deduced (see Tab I). They are found to be $\nu_* \simeq 0.83$ and $K \simeq 1$ respectively, weakly dependent on the rotating speed Ω [40]. The reference temperature field $T_{ref}(x, z) = -z\cos\theta/K$ is then known.

Ω	2 rpm	4 rpm	5 rpm	6 rpm	10 rpm	15 rpm
ν_*	0.84	0.86	0.84	0.82	0.83	0.82
K	0.4	0.8	1.1	1.1	1	0.8

TABLE I: Variation of the reference volume fraction ν_* and the parameter K involved in the state Eq. 2 with respect to the rotating speed Ω of the drum. They are found to be $\nu_* \simeq 0.83$ and $K \simeq 1$ respectively, weakly dependent on the rotating speed Ω [40].

The knowledge of both the field $T(x, z)$ and $\psi(x, z)$ allows to check the first prediction (first equation in system 21) of the approach derived in Sec. II. Figure 5a shows $T(x, z)$ as a function of $\psi(x, z)$ for $\Omega = 6$ rpm. The points clearly gather along a single function. It is worth to emphasize that such result would have been trivial in homogeneous flows such as the observed in Couette geometry or inclined plane geometry: in such flows, all the continuum quantities depend on a single spatial co-ordinate and are thus naturally related two by two by single functions. On the other hand, the fact that the 2D fields $T(x, z)$ and $\psi(x, z)$ can be related by a *single* function in the inhomogeneous surface flow considered here, where the continuum quantities depend on the *both* two spatial coordinates x and z, is highly non trivial and constitutes then a rather severe test for the approach derived in Sec. II. The function F (red thick line in Fig. 5a) is then defined by averaging the values T falling into logarithmically distributed bins defined along ψ. The functions F obtained using this procedure for the various rotating speeds Ω are represented in Fig. 5b.

One can now determine the second closure relation $G(\psi)$. The function $F(\psi)$ defined in the previous section (red thick line in Fig. 5a) is first derived numerically. The resulting function is then applied in each point (x, z) to the field $\psi(x, z)$. Since the reference temperature $T_{ref}(x, z) = -z\cos\theta/K$ and the vorticity field $q(x, z)$ are also known in each point, one can deduce the value of the field $q(x, z) + KF'(\psi(x, z))\log T_{ref}(x, z)$ in each point, and plot it as a function of $\psi(x, z)$ (see Fig. 6a). The points clearly gather along a single function. The function G (red thick line in Fig. 6a) is then defined by averaging the values $q(x, z)/KF'(\psi(x, z))\log T_{ref}(x, z)$ falling into logarithmically distributed bins defined along ψ. The functions G obtained using this procedure for the various rotating speeds Ω are represented in Fig. 6b.

D. Discussion of the results

Our determination of the two closure functions calls for some comments. A first noticeable feature is that the closure function extends smoothly, without any noticeable transition, from the static to the flowing region. This is quite remarkable, since both phases are characterized by different dynamical properties, and since our hydrodynamic description presumably applies best within the flowing region. The main difference between the two

phases is in the scattering of the data along the fit: It is larger in the flowing region than in the static region. This may be traced to correlated fluctuations that have been neglected in our approach, see after Eq. 15, and that are larger in the flowing region. It would be interesting to see if a longer time averaging leads to a reduction of this scattering.

An interesting comparison can also be made with respect to a real fluid system, where a similar approach can be used and where dissipation is made through ordinary viscosity. In that case, it has been shown in [25] that the determination of the closure function is valid only in the bulk flow region. Outside this region, the data scatters randomly, without forming any specific shape. A possible explanation was that outside the bulk, i.e. closer to the boundaries and the flow forcing devices, viscous and forcing processes become important and do not balance *locally* on average as assumed here. The reason why it works so well in the granular case, without any need of selecting any flow region, may lie in the local character of the dissipative processes that precludes any long-range correlation between forcing and dissipation.

IV. CONCLUDING DISCUSSION

In this paper, the stationary states of a rotating dense inhomogeneous granular flow have been shown to be characterized by two functions F and G linking the granular temperature, vorticity and stream functions. When varying the rotation speed of the apparatus, both F and G vary, so that they can be seen as representative of the state of the system. Conversely, the knowledge of F and G is sufficient to fully reconstruct the 2D fields for temperature and velocity. Let us first consider the flowing phase. From Fig. 5 and Fig. 6, one sees that, in that phase, F is asymptotically linear $F \sim a\psi$, while G is approximately constant, $G \sim b$. Inserting these shapes in eq. (21) leads to:

$$\begin{aligned} \delta T &= a\psi, \\ \Delta\psi &= -aK \log(-z\cos\theta/K) + b \end{aligned} \tag{24}$$

Integrating the second equation with respect to z, one finds:

$$\psi = (b - aK\log(\cos\theta/K))\,\frac{z^2}{2} + \frac{3}{2}aKz - \frac{aK}{2}z^2\log(-z) \tag{25}$$

so that the temperature profile is quadratic, with logarithmic correction and the velocity profile is linear, with logarithmic correction. This is indeed the behaviour observed in this type of flow in the flowing phase [6, 11, 26, 28].

In the static phase, F appears quadratic in ψ , $F \sim c\psi^2$ and G is linear $G \sim d\psi$. Therefore, eq. (21) becomes:

$$\begin{aligned} \delta T &= c\psi^2, \\ \Delta\psi &= (d - 2cK\log T_{ref})\psi \end{aligned} \tag{26}$$

The solution for ψ is in this case

$$\begin{aligned} \psi &= \psi_0 \exp(h(z)), \\ h'^2(z) + h''(z) &= d - 2cK\log T_{ref} > 0, \end{aligned} \tag{27}$$

so that both the velocity profile and the temperature profiles are exponential, with algebraic corrections. This is indeed the behaviour observed in the static phase of the rotating drum [28, 41, 42].

These simple asymptotics show the importance of understanding the shape of F and G as a function of the forcing and dissipation. From an experimental or numerical point of view, one may try and find empirical laws from variation of the control parameters like rotation speed, size of the beads, friction coefficient, etc. From a theoretical point of view, one could try to link these functions to the macroscopic flow geometry and the microscopic properties of the flow or rheology through kinetic equations. In a next paper, we explore an alternate strategy, based upon the statistical mechanics Jaynes' interpretation in term of information theory. This will lead to Gibbs distributions providing a direct link between the function F and G and the fluctuations of physical quantities. In this respect, the present approach provides a useful insight for dense granular flow.

Acknowledgments

We gratefully acknowledge O. Dauchot for a critical reading of the manuscript. Simulations are performed using LMGC90 software. This work is supported by the CINE (*Centre d'Information National et d'Enseignement*) under the project lmc2644. We are grateful to S. Aumaitre, O. Dauchot, F. Leschenault and R. Monchaux for many enlightening discussions.

[1] H. M. Jaeger, S. R. Nagel, and R. P. Behringer, "Granular solids, liquids, and gases", Reviews of Modern Physics **68**, 1259 (1996).

[2] S. B. Savage and D. J. Jeffrey, "The stress tensor in a granular flow at high shear rates", J. Fluid Mech. **110**, 255 (1981).

[3] J. T. Jenkins and S. B. Savage, "A theory for the rapid flow of identical smooth inelastic, spherical particle", J. Fluid Mech. **130**, 187 (1983).

[4] C. K. K. Lun and S. B. Savage, "The effect of an impact dependent coefficient of restitution on stresses developed by sheared granular materials", Acta Mech. **63**,

15 (1986).
[5] R. Nedderman, *Statics and Kinematics of Granular Materials* (Cambridge University Press, Cambridge,England, 1992).
[6] G.D.R. Midi, "On dense granular flows", Eur. Phys. J. E **14**, 341 (2004).
[7] P. Mills, D. Loggia, and M. Texier, "Model for stationary dense granular flow along an inclined wall", Europhys. Lett. **45**, 733 (1999).
[8] B. Andreotti and S. Douady, "Selection of velocity profile and flow depth in granular flows", Phys. Rev. E **63**, 031305 (2001).
[9] J. T. Jenkins and D. M. Hanes, "Kinetic theory for identical, frictional, nearly elastic spheres", Phys. Fluids **14**, 1228 (2002).
[10] D. Bonamy and P. Mills, "Diphasic-non-local model for granular surface flows", Europhys. Lett. **63**, 42 (2003).
[11] J. Rajchenbach, "Dense rapid flow of inelastic grains under gravity", Phys. Rev. Lett **90**, 144302 (2003).
[12] S. B. Savage, "Analysis of slow high concentration flows of granular materials", J. Fluid Mech. **377**, 1 (1998).
[13] L. Bocquet, W. Losert, D. Schalk, T. Lubensky, and J. Gollub, "Granular shear flow dynamics and forces: Experiment and continuum theory", Phys. Rev. E **65**, 01307 (2002).
[14] L. S. Mohan, K. K. Rao, and P. R. Nott, "Frictional cosserat model for slow shearing of granular materials", J. Fluid Mech **457**, 377 (2002).
[15] I. S. Aranson and L. S. Tsimring, "Continuum theory of partially fluidized granular flows", Phys. Rev. E **65**, 061303 (2002).
[16] O. Pouliquen and R. Gutfraind, "Stress fluctuations and shear zones in quasi-static granular flows", Phys. Rev. E **53**, 552 (1996).
[17] G. Debregeas and C. Josserand, "A self-similar model for shear flows in dense granular materials", Europhys.Lett. **52**, 137 (2000).
[18] O. Pouliquen, Y. Forterre, and S. L. Dizes, "Slow dense granular flows as a self induced process", Adv. Complex System **4**, 441 (2001).
[19] A. Lemaitre, "The origin of a repose angle: Kinetic rearrangement for granular materials", Phys. Rev. Lett. **89**, 064303 (2002).
[20] I. Iordanoff and M. M. Khonsari, "Granular lubrication: Toward an understanding of the transition between kinetic and quasi-fluid regime", ASME J. Tribol. **126**, 137 (2004).
[21] F. D. Cruz, S. Eman, M. Prochnow, . J.-N. Roux, and F. Chevoir, "Rheophysics of dense granular materials: Discrete simulation of plane shear flows", Phys. Rev. E **72**, 021309 (2005).
[22] P. Jop, Y. Forterre, and O. Pouliquen, "A constitutive law for dense granular flows", Nature **441**, 727 (2006).
[23] N. Leprovost, B. Dubrulle, and P.-H. Chavanis, "Thermodynamics of magnetohydrodynamic flows with axial symmetry", Phys. Rev. E **71**, 036311 (2005).
[24] N. Leprovost, B. Dubrulle, and P.-H. Chavanis, "Dynamics and thermodynamics of axisymmetric flows: Theory", Phys. Rev. E **73**, 046308 (2006).
[25] R. Monchaux, F. Ravelet, B. Dubrulle, A. Chiffaudel, and F. Daviaud, "Properties of steady states in turbulent axisymmetric flows", Phys. Rev. Lett. **96**, 124502 (2006).
[26] M. Renouf, D. Bonamy, F. Dubois, and P. Alart, "Numerical simulation of two-dimensional steady granular flows in rotating drum: On surface flow rheology", Phys. Fluids **17**, 103303 (2005).
[27] J. Rajchenbach, "Granular flows", Adv. Phys. **49**, 229 (2000).
[28] D. Bonamy, F. Daviaud, and L. Laurent, "Experimental study of granular surface flows via a fast camera: A continuous description", Phys. Fluids **14**, 1666 (2002).
[29] D. Bonamy, F. Daviaud, L. Laurent, and P. Mills, "Texture of granular surface flows: experimental investigation and biphasic non-local model", Gran. Matt. **4**, 183 (2003).
[30] P. Jop, Y. Forterre, and O. Pouliquen, "Crucial role of side walls for granular surface flows: Consequences for the rheology", J. Fluid Mech. **541**, 167 (1990).
[31] R. J. Speedy, "Glass transition in hard disc mixtures", J. Chem. Phys. **110**, 4559 (1999).
[32] P.-H. Chavanis and J. Sommeria, "Thermodynamical approach for small-scale parametrization in 2D turbulence", Phys Rev. Lett. **78**, 3302 (1997).
[33] P.-H. Chavanis and J. Sommeria, "Statistical mechanics of the shallow water system", Phys Rev. E **65**, 026302 (2002).
[34] J.-J. Moreau, in *Non Smooth Mechanics and Applications, CISM Courses and Lectures*, edited by J.-J. Moreau and e. P.-D. Panagiotopoulos (1988), vol. 302 (Springer-Verlag, Wien, New York), pp. 1–82.
[35] M. Jean, "The non-smooth contact dynamics method", Comp. Meth. Appl. Mech. Engrg **177**, 235 (1999).
[36] M. Renouf and P. Alart, "Conjugate gradient type algorithms for frictional multicontact problems: Applications to granular materials", Comp. Meth. Appl. Mech. Engrg. **194**, 2019 (2004).
[37] M. Renouf, F. Dubois, and P. Alart, "A parallel version of the non smooth contact dynamics algorithm applied to the simulation of granular media", J. Comput. Appl. Math. **168**, 375 (2004).
[38] D. Bonamy, F. Daviaud, L. Laurent, M. Bonetti, and J.-P. Bouchaud, "Multi-scale clustering in granular surface flows", Phys. Rev. Lett. **89**, 034301 (2002).
[39] O. Reynolds, "On the dilantancy of media composed of rigid particles in contact", Phyl. Mag. Ser. 5 **20**, 469 (1885).
[40] Strickly speaking, the parameter K is found to be significantly smaller for $\Omega = 2$ rpm. However, for this particular rotating speed, the flowing layer is very small. As a result, the variation range of both $\nu(x, z)$ and $T(x, z)$ are very small, making the fit with Eq. 23 rather imprecise.
[41] T. S. Komatsu, S. Inagasaki, N. Nakagawa, and S. Nasuno, "Creep motion in a granular pile exhibiting steady surface flow,", Phys. Rev. Lett. **86**, 1757 (2001).
[42] S. C. du Pont, R. Fisher, P. Gondret, B. Perrin, and M. Rabaud, "Instantaneous velocity profiles during granular avalanches,", Phys. Rev. Lett. **94**, 048003 (2005).

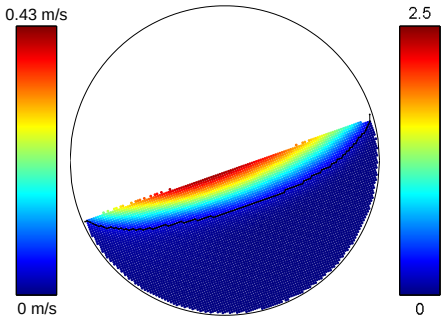

FIG. 1: Time averaged velocity field in the simulated 2D rotating drum. In this peculiar numerical experiment, the rotation speed was $\Omega = 6$ rpm. The black line shows the interface between the flowing layer and the "static" packing. Velocities are expressed in m/s (left-hand colorbar) or non-dimensionalized by $\sqrt{(gd)}$ (right-hand colorbar) where g refers to the gravity constant and d to the mean diameter of the beads (see text for details).

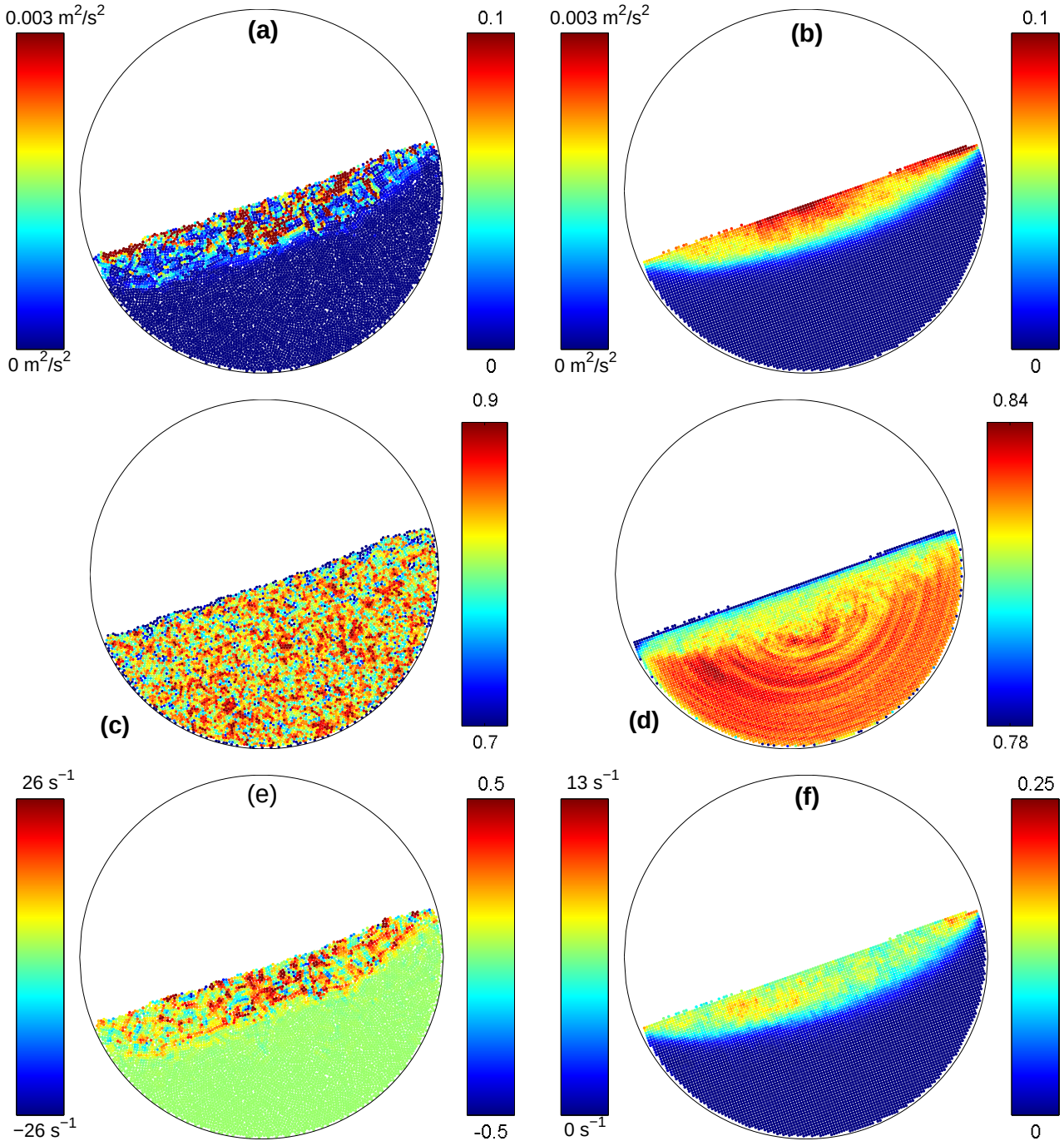

FIG. 2: Spatial dististribution of the various continuous fields measured within the drum. In this peculiar numerical experiment, the rotation speed was $\Omega = 6$ rpm. Left: Typical snapshot of the instantaneous spatial distribution of granular temperature (a), volume fraction (c) and vorticity (e) within the rotating drum. Right: Time averaged field of temperature (b), volume fraction (d) and vorticity (f). The average was taken over the 400 snapshots of the sequence for $\Omega = 6$ rpm. Temperatures are expressed in m^2/s^2 (left-hand colorbar) or non-dimensionalized by gd (right-hand colorbar). Vorticities are expressed in s^{-1} (left-hand colorbar) or non-dimensionalized by $\sqrt{g/d}$ (right-hand colorbar) where g refers to the gravity constant and d to the mean diameter of the beads (see text for details).

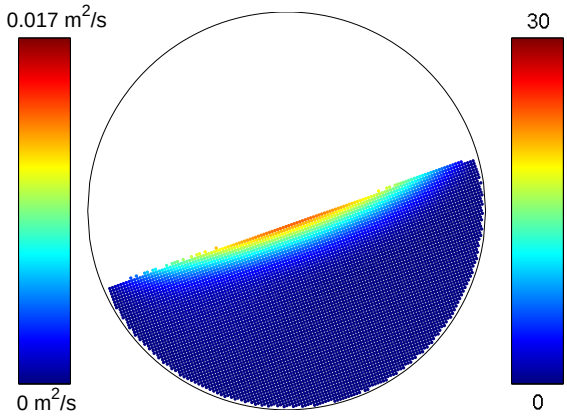

FIG. 3: Spatial distribution of the stream function ψ in the drum for $\Omega = 6$ rpm. The stream function is expressed in m^2/s (left-hand colorbar) or non-dimensionalized by $d\sqrt{(gd)}$ (right-hand colorbar) where g refers to the gravity constant and d to the mean diameter of the beads (see text for details).

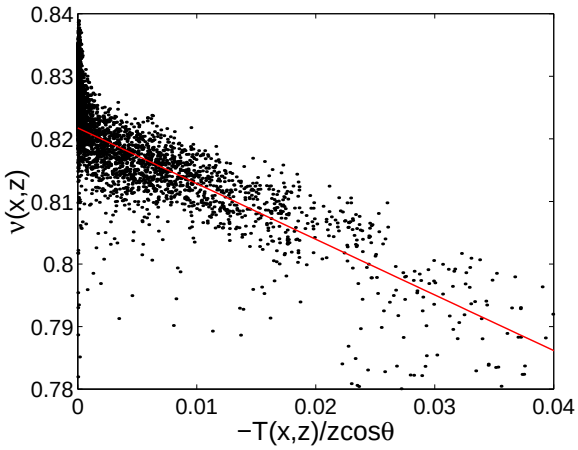

FIG. 4: Volume fraction $\nu(x, z)$ as a function of the ratio $T(x, z)/z \cos\theta$ for $\Omega = 6$ rpm. For this rotation speed, the mean slope of the free surface was measured to be $\theta \simeq 19.7^\circ$ [26]. The straight line is a fit given by Eq. 23 with $K \simeq 1.1$ and $\nu_* \simeq 0.82$. The temperature is non-dimensionalized bygd where g refers to the gravity constant and d to the mean diameter of the beads (see text for details).

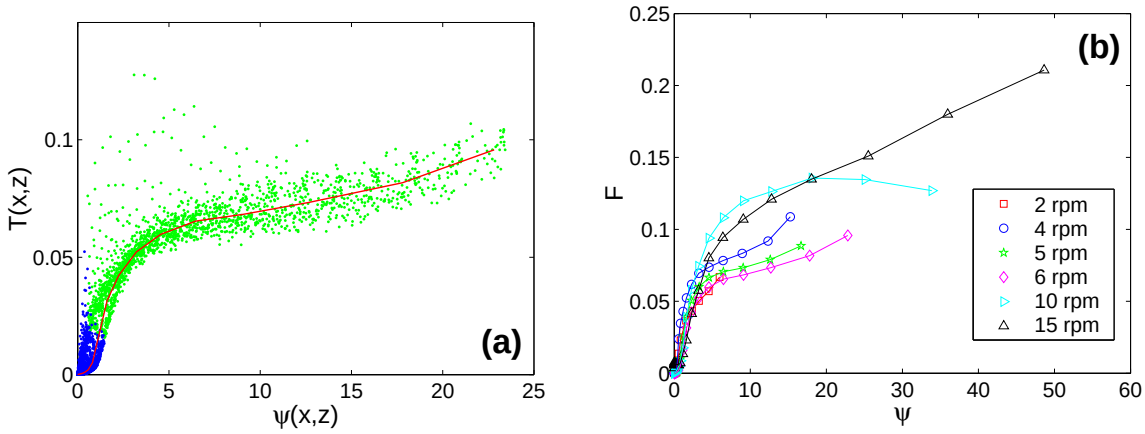

FIG. 5: (a): Variation of the local temperature $T(x,z)$ as a function of the local stream function $\psi(x,z)$ for $\Omega = 6$ rpm. Each dark dot of the cloud corresponds to an elementary square cell $\Sigma(x,z)$ of size equal to the mean bead diameter. Green dots (resp. blue dots) correspond to points that belong to the flowing layer (resp. to the static phase). The red thick line shows the function $\langle T\rangle = F(\psi)$ where $\langle T\rangle$ is defined as the average of the values T of the cells $\Sigma(x,z)$ whose $\psi(x,z)$ fall into logaritmically distributed bins. (b) Variation of $F(\psi)$ as a function of Ω. The temperature and stream function are non-dimensionalized by gd and $d\sqrt{gd}$ respectively, where g refers to the gravity constant and d to the mean diameter of the beads (see text for details).

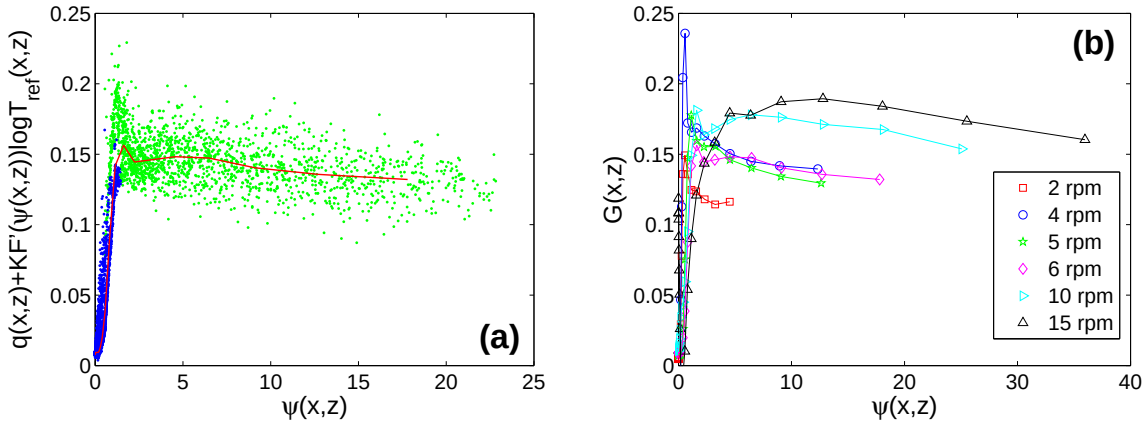

FIG. 6: (a): Variation of the local field $q(x,z) + KF'(\psi(x,z))\log T_{ref}(x,z)$ as a function of the local stream function $\psi(x,z)$ for $\Omega = 6$ rpm. Each dark dot of the cloud corresponds to an elementary square cell $\Sigma(x,z)$ of size equal to the mean bead diameter. Green dots (resp. blue dots) correspond to points that belong to the flowing layer (resp. to the static phase). The red thick line shows the function $\langle q + KF'(\psi)\log T_{ref}\rangle = G(\psi)$ where $\langle\rangle$ is defined as the average on the cells $\Sigma(x,z)$ with values $\psi(x,z)$ which fall into logaritmically distributed bins. (b) Variation of $G(\psi)$ as a function of Ω. The temperature, vorticity and stream function are non-dimensionalized by gd, $\sqrt{g/d}$ and $d\sqrt{gd}$ respectively, where g refers to the gravity constant and d to the mean diameter of the beads (see text for details).